LEX LOCALIS-JOURNAL OF LOCAL SELF-GOVERNMENT
ISSN:1581-5374 E-ISSN:1855-363X
VOL. 24, NO. 2(2026)

COATI-OPTIMIZED BI-LSTM FOR ZERO NDZ ISLANDING DETECTION FOR HYBRID SOLAR-WIND SYSTEMS IN PUBLIC SECTOR

[*1]Bindu Vadlamudi, [2]T. Anuradha

[*1]Research Scholar, EEE Research Centre, KCG College of Technology, Chennai, Tamil Nadu, 600097 India.
[2]Department of Electrical and Electronics Engineering, KCG College of Technology, Chennai, Tamil Nadu, 600097 India.

[*1]bindu.vadlamudi@gmail.com,
[2]anuradha.eee@kcgcollege.com

Abstract
The biggest issues prevailing in managing microgrids is the potential for unintentional islanding. This can result in critical risk exposure and technological problem. In these situations, locating and recognizing the defect is essential to equipment maintenance and protection. There are drawbacks to many of the works used in the literature, such as longer tripping times and larger non-detection zones (NDZ). To address these problems, a classifier based on green anaconda optimization with bi-directional long short-term memory (Bi-LTSM) and Fourier Bessel series expansion (FBSE) with empirical wavelet transform (EWT) is proposed. A modified Institute of Electrical and Electronics Engineers (IEEE) 33 bus distribution network with solar and wind integration is used to validate this work on the MATLAB/Simulink platform. Several distribution network defects, such as motor starting, nonlinear load, capacitor bank switching, islanding conditions, etc., are been used to identify islanding. The output gives that proposed method correctly identifies islanding activities and acts correctly in every other situation. According to simulation data, the proposed approach may identify the islanding process in less than 75 milliseconds. The original dataset with zero NDZ delivers 100% accuracy, the proposed approach with the noisy dataset produces an average accuracy of 99.95%.

Keywords: Distributed generation (DG), hybrid solar-wind, Wavelet transform-based self-organizing mapping network (WT-SOMN), distributed WT-based artificial neural network (DWT-ANN), convolutional NN-based LSTM (CNN-LSTM) and dual-tree complex WT-based support vector machine (DTCWT-LSTM)

1. Introduction

Recently, distributed energy resources have become increasingly popular due to their importance in meeting load demands. Distributed generation (DG) typically involves small generation units, including mini-hydro turbines, wind farms, geothermal, fuel cell, biomass and solar energy [1]. Idea of a microgrid was also developed due to the expansion of DG penetration depth and existence near electricity. Two operating modes of microgrids are grid-connected and islanded condition. Here when the system is operated under grid connected mode, the primary utility based on microgrid [2]. DG units that make up microgrid are managed and operated using power control mode like "Grid Following". Microgrid operates independently of the main power grid and controls its voltage and frequency. When an electrical area can operate independently of the rest of the power grid, a microgrid is created [3].

In the islanded state, a part of a distributed network is not connected to the grid but still receives electricity from one or more connected DG units. The main technical issue caused by DG connected to the electricity system is unintentional islanding. Based on the IEEE standard, all sources should be disconnected within two seconds of an islanding [4]. Numerous islanding detection methods were created and reported in various categories, such as remote and local methods. In a local technique, the measurement is done at the DG side, while in a remote technique, the measurement is done at the utility side. The NDZ measures the effectiveness of each method [5]. Some passive techniques for NDZ reduction and improvised work on island detection are based on state-of-the-art intelligence and signal processing techniques [6]. Techniques that have been developed include fuzzy logic, random forest classifiers, decision

trees and naive Bayes classifiers. S-transform, Wavelet transform and wavelet packet transform are schemes proposed by the authors [7]. However, all these methods have some delays, such as slow detection of NDZ, low power quality, harmonic limit, difficult to implement, etc. Several techniques for detecting islanding in microgrids are discussed in the literature. One of the important problems in passive island detection is the large NDZ. In addition, active methods involve the issue of power quality. This paper uses neural network technology with islanding detection techniques. The main objectives of the method are given below;

- To reduce NZD zone, FBSE-EWT-based GAO-optimized Bi-LSTM method is proposed.
- To extract the features from PCC under islanding detection conditions, FBSE-EWT is used.
- The classification task is performed under islanding conditions using the GAO-optimized Bi-LSTM method.
- For validation purposes, the proposed islanding detection technique is simulated using a modified IEEE 33bus system with two distribution generator units.

This work is classified into five sections: Section 1 introduces detection of islanding and contribution. Issues related to the islanding in existing works are discussed in section 2. The proposed methods with feature extraction and classification approaches are covered in section 3. Results of the proposed method, along with existing approaches, are compared and discussed in section 4. The conclusion of the proposed work and results are given in section 5.

2. Related Works

In the work, the traditional methods on islanding detection using different methods are discussed. For a grid-connected photovoltaic system, Bakhshi-Jafarabadi et al. [8] suggested a fast and accurate detection of islanding method. This method regulates the active power output by injecting a disturbance, such as the absolute deviation of the output voltage, into the inverter's d-axis reference current. When operating in an island manner, disturbance diminishes active output power, therefore, voltage at common coupling point above desired value. Elshrief et al. [9] offered a hybrid passive-active systematic method based on an intelligent classifier. In this method, three ports were used to measure reactive power: load port, grid port and DG port. These three reactive power values are a basis for the fuzzy system to make decisions.

Ashwin et al. [10] suggested a passive islanding detection with the dwarf mongoose optimization method and the random forest algorithm. This method of identifying and categorizing island and non-island events in DGS uses three key areas, namely feature extraction, dataset generation and classification. Naraghipour et al. [11] suggested a Q-f droop curve technique in inverter based distributed generator. The suggested method uses delivered reactive power as the input of the converter. This method is verified with the motor to improve island detection performance. Using this suggested method, the dynamic load was disconnected from the circuit automatically during the fault. Pangedaiah et al. [12] introduced a passive islanding detection technique using second generation WT (SGWT) and maximum overlap discrete WT (MODWT). In this method, MODWT distributes the scale coefficient and the frequency spectrum. SGWT reduces the computation time to 0.3 s under the condition that there is no performance mismatch. In previous work, the features were extracted by the Fourier and short-time Fourier transforms, which have low time-frequency resolution. However, the intelligent classifiers are used for training the model for islanding detection. Deep learning-based classifiers are more efficient when processing large numbers of voltage waveform samples retrieved from signal processing processes. Hence, the proposed work is intended to design an intelligent method for designing the feature extraction method with a classifier to get a zero non-detection zone.

3. Proposed methodology

In this work, the important features of a hybrid solar-wind connected system are gathered by an FBSE-EWT under different faulty conditions. At the same time, the neural network models are more efficient for processing plenty of data. Hence, the Bi-LTSM is used in this work for islanding detection. The Bi-LTSM is used to classify islanding events based on extracted features. GAO Algorithm is used to tune the weights of Bi-LSTM. The proposed system is estimated under several possible events to capture important features of system for training and testing. NDZ is the condition in which islanding systems cannot identify the islanded state. The proposed methodology is validated for a zero NDZ. The proposed method will be validated on a modified IEEE 33 distribution bus system. Figure 1 represents a block diagram for the proposed work.

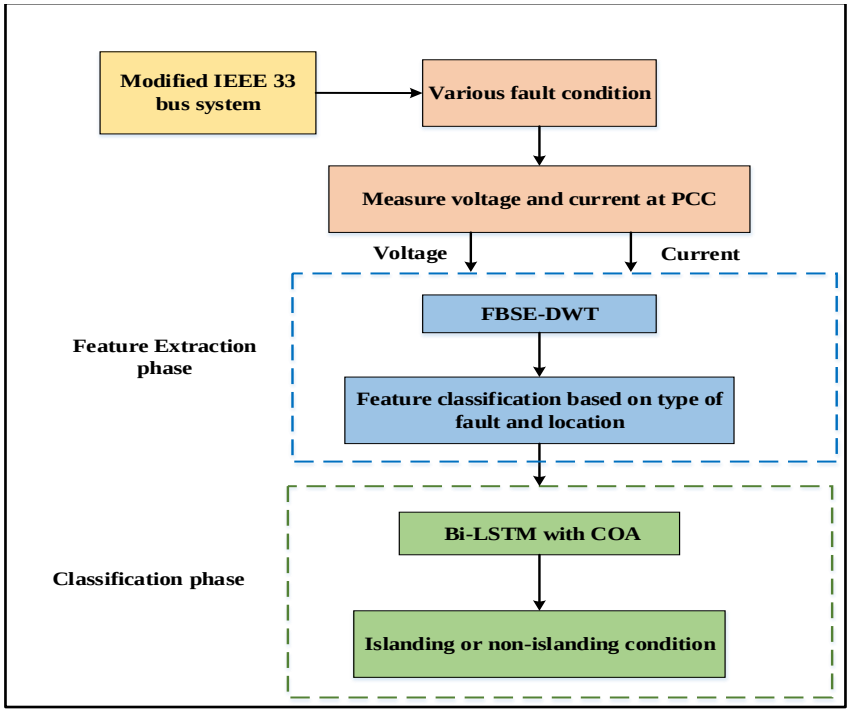

Figure 1: Block diagram for proposed work

3.1 Modified IEEE 33 bus system

The initial design of 33 bus consisted of 33 buses, 32 fixed and 5 switchable lines, and no reactive power balancing devices [21]. Power to the network is fed via a feeder connected to the first bus. The voltage of buses is between 0.9 and 1.1 (p.u.). A modified IEEE bus system is used to interconnect additional sources and loads. PV, wind, capacitors, induction motors and additional loads are connected in the proposed bus. In this work, sources like PV and wind are connected in bus numbers seven and twenty-five, respectively. In addition, the bus system was divided into five zones to evaluate the location of the fault. The line diagram for the modified IEEE-33 bus is presented in Figure 2.

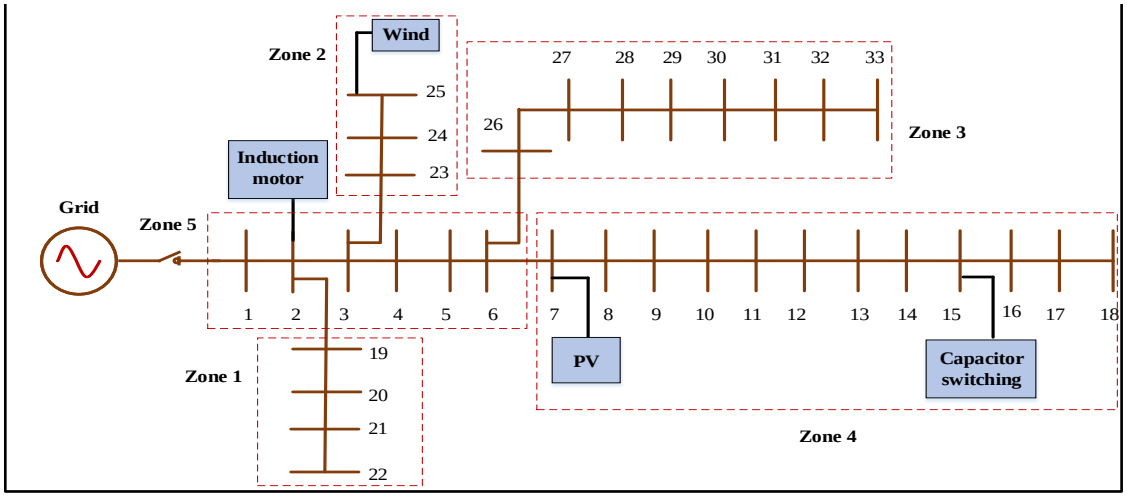

Figure 2: Modified IEEE-33 test system

3.1.1 Modelling of solar PV

Solar photovoltaic (PV) systems operate based on the irradiance, where incident solar radiation is directly converted into electrical energy. PV generation is clean, renewable and increasingly cost-effective due to technological advancements and large-scale manufacturing. The electrical output of a PV module is influenced by several factors and operational environment such as irradiance, temperature and electrical load connected to the system. Typically, a PV module is constructed by interconnecting various batteries in series to increase voltage and in parallel to increase current. For analytical and simulation purposes, a single-diode model is widely used since it provides a good balance between accuracy and computational simplicity.

$$I = I_{Ph} - I_d\left[\exp\left(\frac{(V + I.R_S)}{V_{th}\lambda}\right) - 1\right] - \frac{(V + I.R_S)}{R_P} \quad (1)$$

Here, I denotes output current, λ indicates identity factor, I_d signifies diode current, I_{Ph} denotes photo-generated PV current, V_{th} is the thermal voltage. Where V represents output voltage, R_{series} and R_{shunt} are solar cells in series and parallel resistance respectively [14].

3.1.2 Modelling of wind turbine

Wind energy generation depends directly on the velocity of the incoming wind, that drives the turbine blades the kinetic energy into electrical power. Since wind speed fluctuates continuously, the electrical output of a wind turbine also varies. The actual power produced at any instant are by the wind speed that measured at the hub height, along with specific turbine characteristics and operating limits. The electrical power extracted from the wind can be expressed mathematically as:

$$P_W = \begin{cases} P_{Rated} & ;V_{Rated} \le V_W \le V_{CO} \\ P_{Rated} \times \left(A \times V_W^3 - B\right) & ;V_{CI} \le V_W \le V_{Rated} \\ 0 & ;Otherwise \end{cases} \quad (2)$$

Where, P_{Rated} indicates rated wind power, P_W represent wind power output, A implies the area of wind plant and B indicates constant coefficient. The rated speed of the wind, actual

speed of wind, cut-out and cut-in speed of wind turbine are represented as V_{Rated}, V_W, V_{CO} and V_{CI} respectively [15].

3.1.3 Loads

Local load generates an equivalent P_{load}, Q_{load} demand at the PCC with a specified quality factor Q_f, which represent the proportion of system energy to the energy dissipated over a particular period.

$$P_{load} = \Delta P + P_{DG} \tag{3}$$

$$Q_{load} = \Delta Q + Q_{DG} \tag{4}$$

Where, P_{load}, P_{DG} and ΔP represent active power in load, distributed system and change in active power, respectively. Q_{DG}, Q_{load} and ΔQ indicates reactive power for distributed sources, load and change in reactive power, respectively. In order to simulate step changes in demand, the load can be changed by adding parallel RLC, which can test the robustness of islanding detection against wrong detections [16]. A three phase squirrel cage induction motor is coupled as a load to a modified IEEE 33 bus system. Because their construction is completed without slip rings, induction motors are comparatively inexpensive and durable equipment. The primary voltage frequency and the number of poles of the motor were used to control the speed at which induction motors can operate.

3.2 Fourier-Bessel Series Expansion based empirical wavelet transform

The adaptive methodology such as FBSE-EWT evaluate the non-stationary region, consists of two signal processing methods: FBSE and EWT. A non-stationary Bessel function is the basis for the FBSE signal processing technique, making it better suited for analyzing time-varying signals like electroencephalogram, electrocardiogram, etc. EWT is based on adaptive wavelet based filters. The FBSE-EWT technique are utilized in this investigation for separate islanded signals from the individual fault condition signals. Bessel functions are non-stationary and are used as a basis in the FBSE. Because of this, FBSE can analyze signals with time-varying characteristics. Zero order Bessel functions are used to express FBSE of $X(n)$.

$$X(n) = \sum_{M=1}^{m} A_m \, J_0\left(\frac{\beta_m N}{M}\right), \qquad N = 0,1,2,.....M-1 \tag{5}$$

Where, $X(n)$ represent the frequency spectrum of a signal within a range of $[0,\pi]$ frequency, which is achieved by using the FBSE method [17]. The coefficient of the signal $X(n)$ is indicated as A_m, which is measured as follows.

$$A_m = \frac{2}{M^2\left(J_1(\beta_m)\right)^2} \sum_{N=0}^{M-1} N X(n) J_0\left(\frac{\beta_m N}{M}\right) \tag{6}$$

Where, J_1 and J_0 indicates first and zero-order Bessel function. Positive roots of J_0 are organized in ascending order and is represented as β_m, where $m = 1,2,3,.....,M$. The m^{th} order of FBSE coefficients is expressed in terms of the appropriate continuous frequency f (Hz).

$$\beta_m \approx \frac{2\pi f M}{S_{rate}} \tag{7}$$

$$m \approx \frac{2 f M}{S_{rate}} \tag{8}$$

Where, S_{rate} indicates sampling rate in frequency and M represent equal length of the signal. Total bandwidth for m should differ from 1 to M. Between frequency (f) and absolute value coefficient (A_m), the FBSE spectrum is plotted. After fragmenting the fault waves, wavelet and empirical scaling functions are utilized to design a filter based on Littlewoods-Paley and Meyer's wavelet. Based on collected subband signals at different error frequencies, features are extracted from FBSE-EWT.

3.3 Classification based on GAO-optimized Bi-LSTM

A Bi-LSTM is created by combining an LSTM with a bidirectional recurrent neural network. The Bi-LSTM model captures long-range dependencies more effectively by processing data in any orders. This bidirectional structure permits it to utilize past and future contextual, resulting in improved sequence learning. Bi-LSTM networks demonstrate strong classification capabilities and are capable of retaining information over extended durations through their linear memory cells [18]. Each memory block consists of three multiple entry, such as input, output and forget gates, moreover a self-connected memory cells. They are directly mapping Bi-LSTM to hardware, resulting in very low performance. Each neuron must process an additional N input, where N indicates layer of neurons. The forward and reverse transmission status of retrieved load data is assessed using Bi-LSTM.

$$\vec{H}_f = LSTM\left(X_t, \vec{H}_{f-1}\right) \tag{9}$$

$$\overleftarrow{H}_b = LSTM\left(X_t, \overleftarrow{H}_{b-1}\right) \tag{10}$$

$$H_t = W_f \vec{H}_t + W_b \vec{H}_t + C_t \tag{11}$$

In this method $\vec{H}_f$ denotes the hidden layer during forward path, while $\vec{H}_{f-1}$ represent the final cell. $\overleftarrow{H}_b$ corresponds the backward propagation path and $\overleftarrow{H}_{b-1}$ indicates the last cell. C_t refers to the hidden layer bias optimization, W_b depicts the weight matrix at backward propagation and W_f illustrate the output weight parameter. Since the network contains numerous weight parameters, it requires substantial storage capacity along with efficient coordination between memory bandwidth and multiple storage components. For evaluating the GAO algorithm here [19] are employed to set of weight parameters for the Bi-LSTM network.

The GAO algorithm is a nature-inspired metaheuristic technique that simulates the behavioural patterns and movement strategies of green anacondas. It offers an effective balance between exploration and exploitation that make them highly suitable for complex optimization tasks. The proposed method with GAO employed for determining optimal weight parameters in Bi-LSTM network, ensuring improved learning efficiency and accuracy. The initialization population process GAO in expressing equation:

$$X = \begin{bmatrix} X_1 \\ \vdots \\ X_k \\ \vdots \\ X_N \end{bmatrix}_{N\times m} = \begin{bmatrix} X_{1,1} & \cdots & X_{1,D} & \cdots & X_{1,m} \\ \vdots & \ddots & \vdots & \iddots & \vdots \\ X_{k,1} & \cdots & X_{k,D} & \cdots & X_{k,m} \\ \vdots & \iddots & \vdots & \ddots & \vdots \\ X_{N,k} & \cdots & X_{N,D} & \ldots & X_{N,m} \end{bmatrix}_{N\times m} \quad (12)$$

$$\begin{aligned} & X_{k,\,D} = lb_D + r.(ub_D - lb_D) \\ & K = 1,2,\ldots\ldots,N \\ & D = 1,2,\ldots\ldots,m \end{aligned} \quad (13)$$

Here, X indicates GAO population matrix, decision variable is depicted as $X_{i,D}$ in D^{th} dimension, N represent number of data, r represents random number between the interval 0 and 1, X_k indicates candidate solution in k^{th} input data. ub_D indicates upper bound, lb_D signifies lower bound and m signifies the number of decision variables.

Phase 1 (Exploration): female anaconda location are indicated by the weight parameters of BiLSTM that are updated as the male species. Here equation (14) is used to determine the candidate location.

$$FD_k = \{X_{it} : F_{i_k} < F_k \;\; and \;\; i_k \neq k\}, \;\; i_k \in \{1, 2, \ldots\ldots, N\} \quad (14)$$

Here, F_k illustrate the solved value in k^{th} data and F represent the objective. The quality value is updated along every GAO iteration. FD_k denotes the collection of feasible habitat positions for choosing Green Anaconda k^{th} female candidates, whereas i_k specifies the respective row numbers associated with these positions in the matrix. The region of the weight parameter is updated using equation (15)

$$X_{k,D}^{p1} = X_{K,D} + r_{k,D}.(S_D^K - I_{k,D} \cdot X_{K,D}) \quad (15)$$

$$X_k = \begin{cases} X_k^{P1}, & F_k^{P1} < F_k \\ X_k & else. \end{cases} \quad (16)$$

Where, $X_{k,D}^{p1}$ signifies the new suggested position of k^{th} anaconda based on the first phase of GAO, $X_{K,D}$ indicates D^{th} dimension, F_k^{P1} represent objective function value, $r_{k,D}$ are random numbers with a normal distribution in the range of [0, 1], S_D^K denotes D^{th} dimension of selected female for k^{th} green anaconda, $I_{k,D}$ are random numbers from the set {1, 2}.

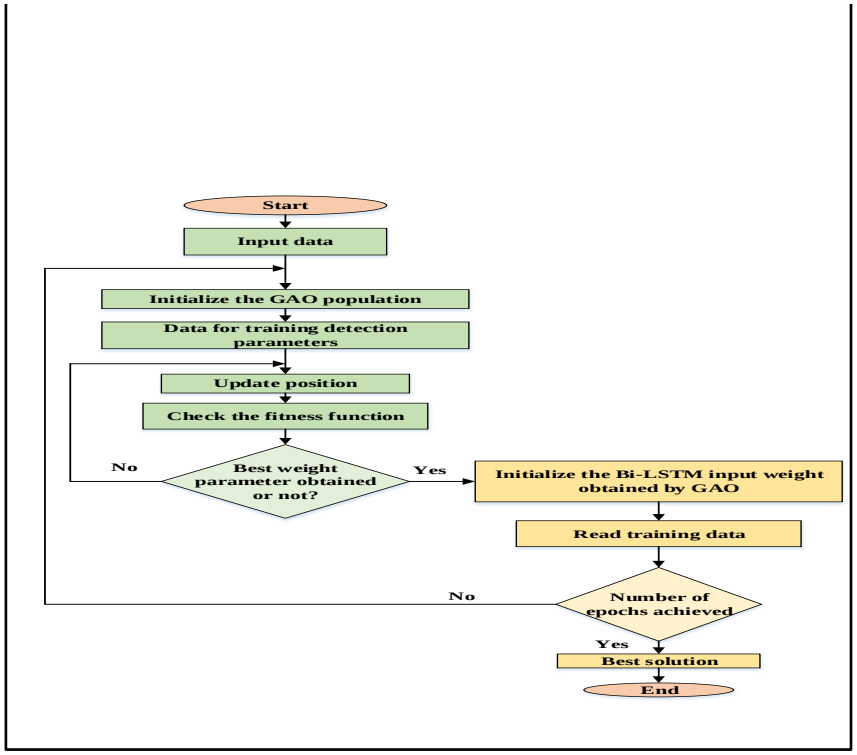

Figure 3: Flowchart for proposed GAO-optimized Bi-LSTM

Phase 2 (Exploitation): The hunting behaviour of the anacondas and the updated new solution is described below,

$$X_{k,D}^{p2} = X_{K,D} + \left(1 - 2R_{k,D}\right)\frac{U_D - L_D}{t} \tag{17}$$

$$X_k = \begin{cases} X_k^{P2}, & F_{ik}^{P2} < F_k \\ X_k & else. \end{cases} \tag{18}$$

Where, $X_{k,D}^{p2}$ denotes updated region k^{th} population and t indicates maximum number of iterations. After updating the position of the anaconda the first iteration cycle. The second phase proceeded with the result obtained from the initial phase. With the updated fitness value and the new position the algorithm advances to the next iteration. In this iteration, best weight parameter is selected so that islanding detection is accurately detected by Bi-LSTM. The flowchart for GAO-based Bi-LSTM are represented as Figure 3.

4. Result and discussion

The results of this work are fault types, fault location and island detection. Here the work is evaluated and compared with the conventional method. Figure 4 shows Simulink model of a modified IEEE 33 bus.

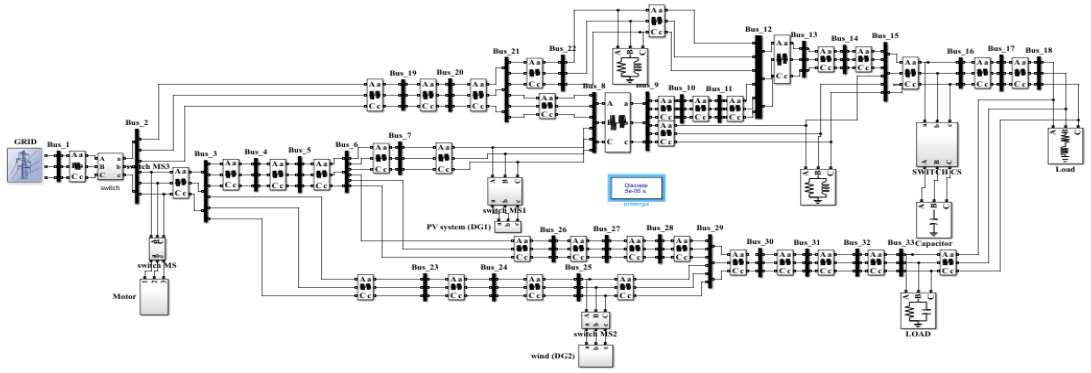

Figure 4: Simulink model

Several types of errors are used in IEEE-33 distributed network. The feature extraction process is provided with voltage and current waveforms for all situations. Using the FBSE-DWT approach, output values for extracted features are calculated and acquired through simulation. A total of 16 types of errors are taken into account in this work; voltage and current are measured on the PCC. Faults applied in both solar and wind-connected bus structures include: without solar source, without wind source, voltage swell, voltage sag, islanding, motor switching, additional load, LLL switching, LL switching, line (L) switching, line-to-ground (LG) stitching, LLG, LLLG, load switching, low-level capacitor and high-level capacitor. The solar system is disconnected from the modified network to check the islanding condition. The grid is simulated for 2 seconds, but the solar is removed between 0.6 to 1.2 seconds. Between these times, voltage and current waveform get slightly decreased. Figure 5 (a) represents the voltage and current waveform in the state of solar source disconnection. The wind energy system is disconnected from distributed system due to fault condition 2. The error occurs between 0.6 and 1.2 seconds, and outputs are recorded with error. Figure 5 (b) shows output devoid of a wind energy source.

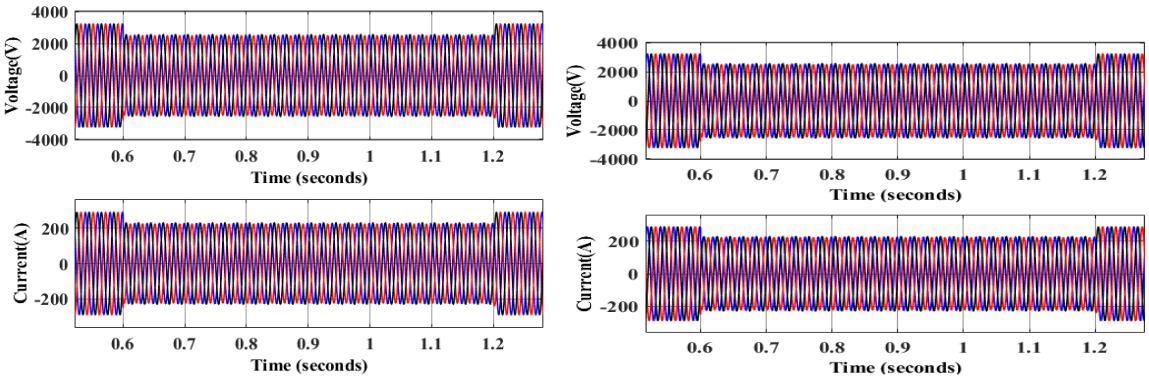

(a) (b)

Figure 5: Characteristic reaction at (a) without DG1 (b) lacking DG2

The modified IEEE bus system is subject to voltage swell condition. In this condition, the voltage is increased from the normal range while the current is decreased from 200A to 25A. Therefore, the error can affect voltage and current between 0.6 and 1.2 seconds. Figure 6 (a) shows output changes during voltage swell. The generating system is subjected to a voltage sag, and the response is evaluated by lowering the voltage. A sag is noticed within two seconds and is caused by an isolated problem in the network method. Figure 6 (b) represent voltage and current appearances of this scenario. The amplitude of voltage waveforms is reduced while the amplitude of current waveforms is increased when a fault arises between 0.6 and 1.2s.

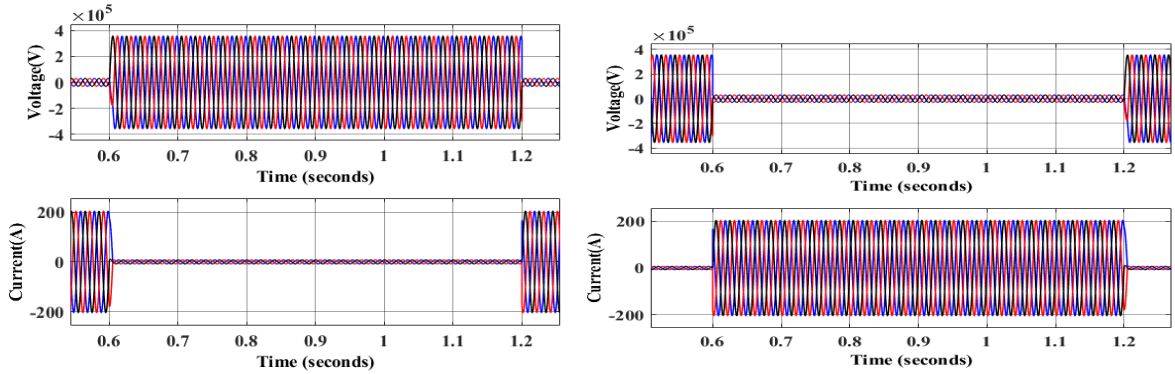

(a) (b)

Figure 6: Simulation response for (a) voltage swell (b) voltage sag condition

Islanding occurs between 0.6 and 1.2 seconds for grid-connected renewable energy sources. Figure 7 shows the transition reaction for an island state. Some distortion has occurred in the voltage waveform at this fault, but in the defective state, the amplitude fluctuates. The current waveform indicates that in the island state, the current remains at zero and in the non-island state, the amplitude remains the same.

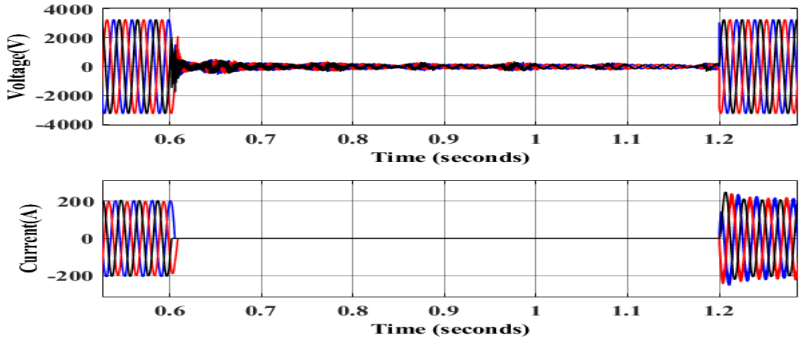

Figure 7: Output of voltage and current at PCC islanding condition

The motor is connected to the second bus in a modified distributed IEEE 33 bus system. For fault number six, the motor switching is used, and outputs are measured at PCC. The output for switching motor is shown in Figure 8 (a). Current and voltage are reduced in this mode due to a fault. Figure 8 (b) represents the output of voltage and current while adding extra load to the distributed system. If additional load is added, the entire circuit will be disturbed. It will reduce the motor operation, and the torque will be increased. It will overheat the circuit when the load is increased normally.

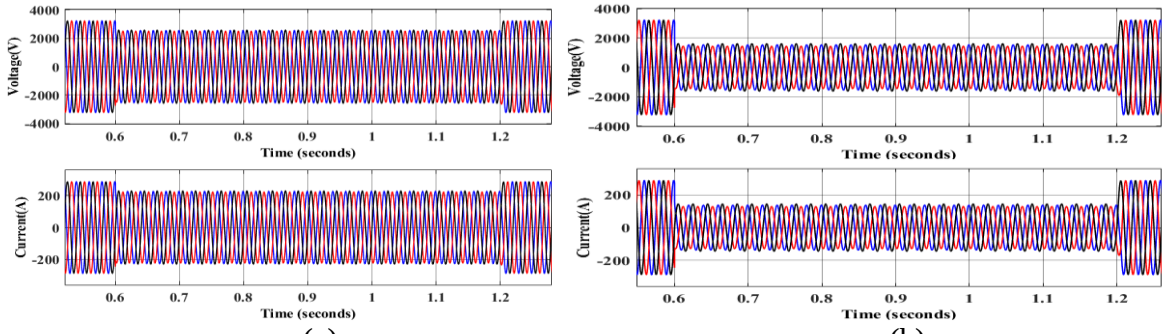

(a) (b)

Figure 8: Waveforms for voltage and current at (a) motor switching (b) adding additional loads.

LLL fault was applied in the modified bus system; this fault is also represented as an unbalanced fault. Since there is an imbalance in the system, a short circuit may occur due to this error. Figure 9 (a) indicates the output of voltage and current in LLL fault condition. This

fault decreases the voltage and increases the current. LL fault is also known as unsymmetrical fault; it will happen when two conductors are short-circuited. Figure 9 (b) shows a three-phase system with an LL fault in two phases. This fault may damage the electrical system; therefore, finding this fault is crucial.

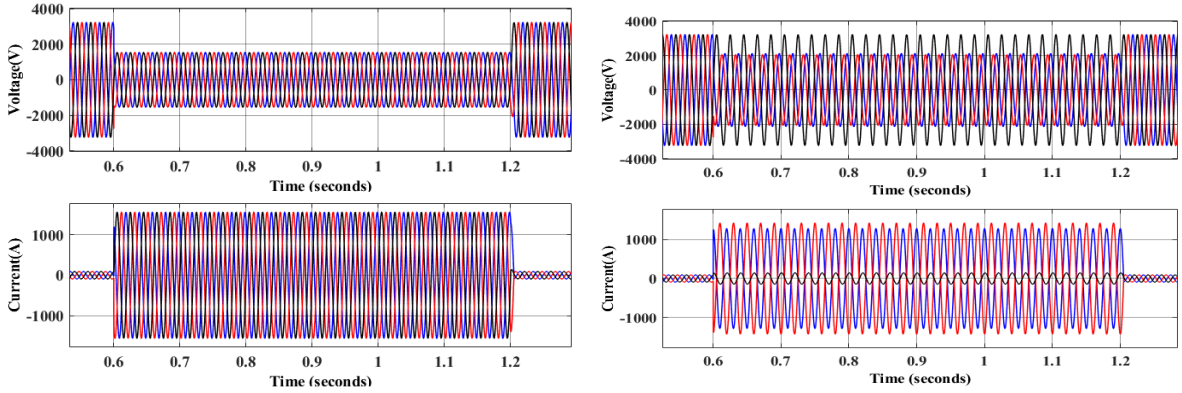

(a) (b)

Figure 9: Characteristic waveform of voltage and current at (a) LLL condition (b) LL fault

Figure 10 (a) indicates the output of voltage and current at load-switching conditions. Power problems occur when switched on and off using integrated load switches. These load switches are additionally added to check the island condition using the proposed method. The ON/OFF state of switches present in the line causes a line switching fault, it is used to investigate the poor status of the power system. The defective situation lasts for 0.6 to 1.2 seconds. The performance of line switching failure is represent Figure 10 (b)

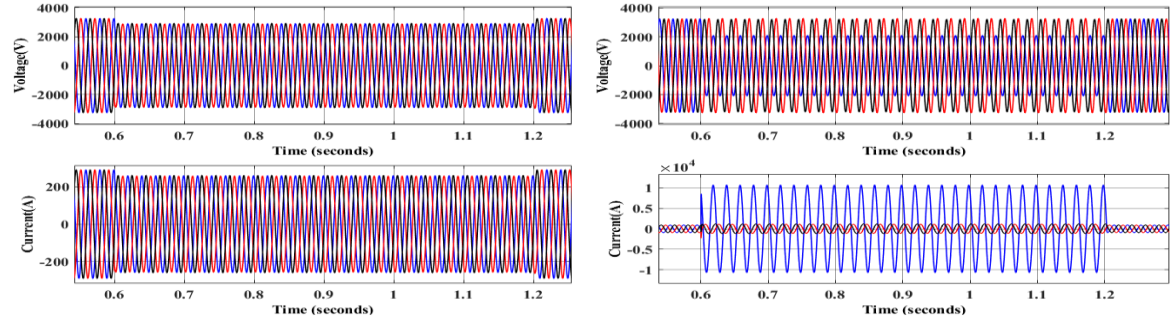

(a) (b)

Figure 10: Simulation results for (a) load switching (b) line switching condition

A single LG failure occurs when one of the power lines makes direct contact with the ground or another low-impedance channel. As a result, an unwanted current flow bypasses the electrical load with safety features and travels from the power line to the earth. Figure 11 (a) shows the output for this case. A double line-to-ground fault is typically represented by a short-circuit connection that involves two phases such as phases A and B, along with their shared junction that is tied to ground through a specified fault resistance. This modeling approach captures the current paths and voltage imbalances characteristic of fault. Figure 11 (b) shows the waveform for this LLG fault condition from PCC. All three phases, A, B, and C, are shorted together and grounded in a fault known as a LLLG fault. It is considered a symmetrical fault, and the output for this fault is given in Figure 11 (c).

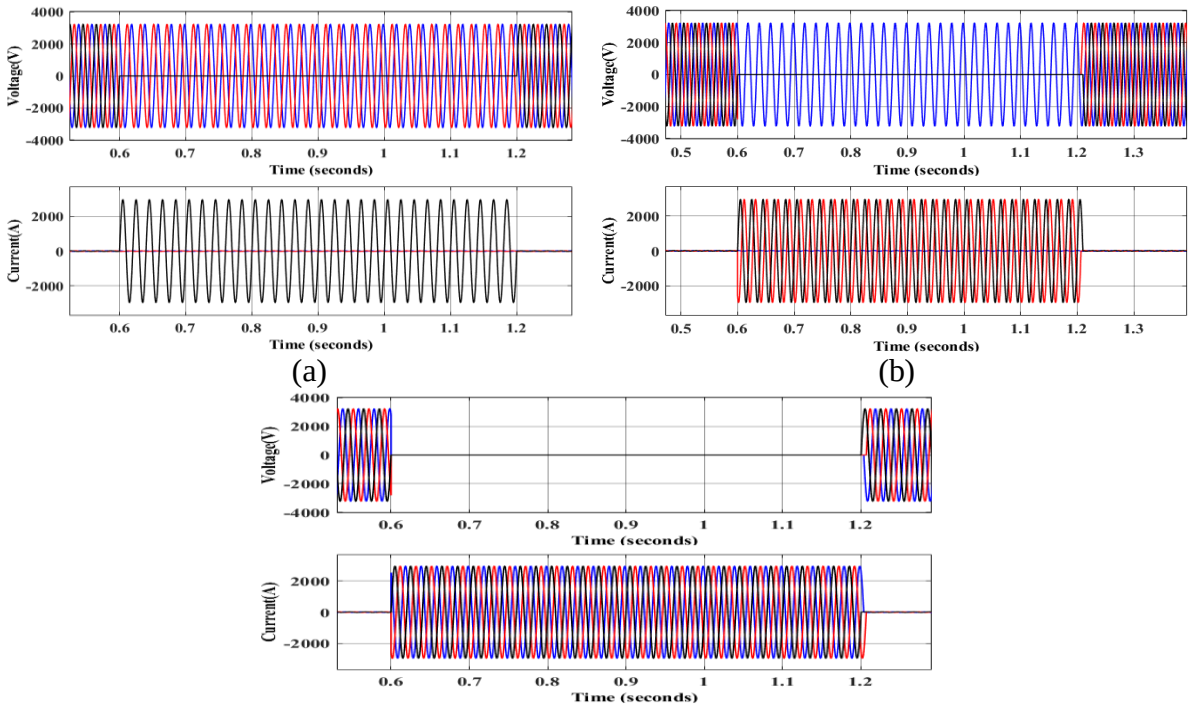

Figure 11: Simulation result for (a) LG fault condition (b) LLG fault (c) LLLG fault

The capacitor helps the motor to start and run smoothly by storing energy and releasing it when needed. If the capacitor fails, the air conditioner may short-circuit or overheat, which could cause a failure. Figure 12 (a) shows the response output for low-level capacitor switching, which will cause a small variation in power. Electrical problems such as undervoltage interruptions may occur due to the ON mode of external machines connected to the network. Figure 12 (b) represents the voltage and current range at a high-level capacitor switching condition.

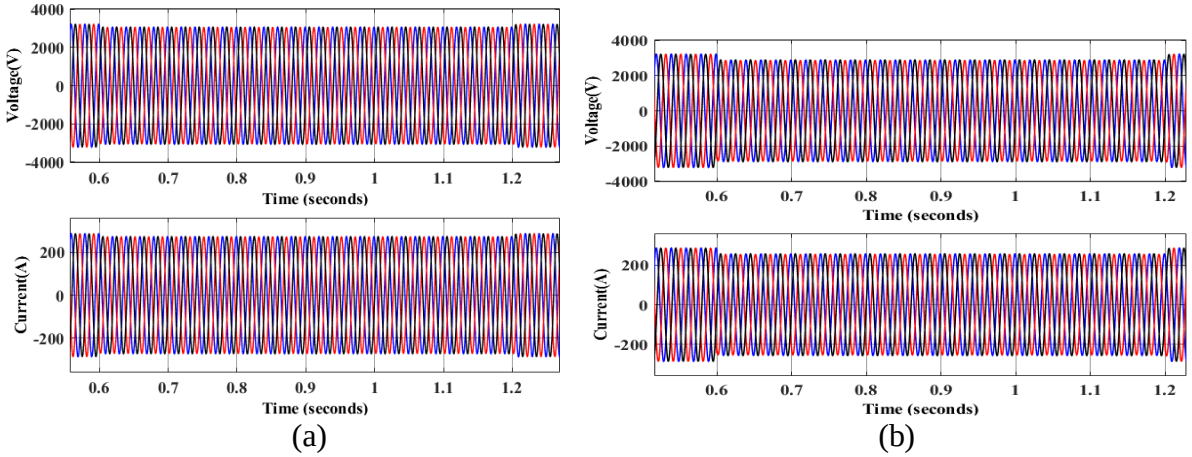

Figure 12: Simulation result for capacitor at (a) low-level switching (b) high-level switching

Figure 13 shows the output of a modified IEEE 33 distribution system without fault conditions or normal conditions. This waveform is used as a reference for finding the fault in other waveforms during the feature extraction process.

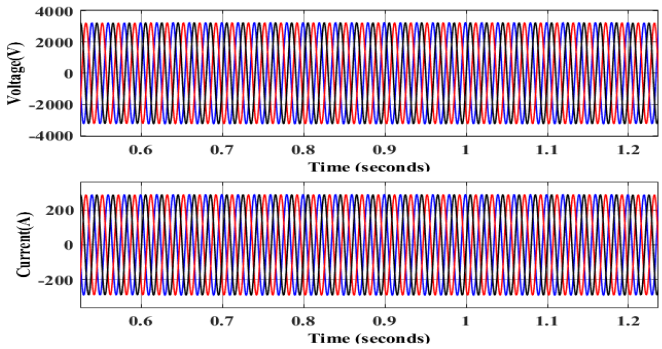

Figure 13: Output of voltage and current at normal state

Proposed method is evaluated based on application of noise in proposed system. In the proposed system, noise levels of 40 dB, 30 dB and 20 dB were applied. Furthermore, performances of proposed method like precision, accuracy, recall, F1 score and specificity is considered for place in evaluation. Table 1 represents the evaluated value for performance analysis like precision, F1-score, recall, specificity and accuracy with and without noise conditions. Values are compared with and without noise conditions to show the efficiency of this method.

Table 1: Comparative analysis of performance metrics with and without noise

Metrics	Without noise	SNR			
		30 dB	40 dB	50 dB	20 dB
Accuracy	1	0.9997	0.9999	0.999	0.997
Precision	99.89	0.9967	0.9987	0.9987	0.9967
Recall	99.95	0.9987	0.9987	0.9987	0.9970
Specificity	99.99	0.9998	0.9998	0.9998	0.9998
F1-Score	99.82	0.9968	0.9987	0.9987	0.9968

Figure 14 indicates a comparative analysis of accuracy in work with conventional methods. For this comparison, islanding detection using different techniques in the IEEE distribution system was considered. Wavelet transform-based self-organizing mapping network (WT-SOMN), a distributed WT-based artificial neural network (DWT-ANN), a convolutional NN-based LSTM (CNN-LSTM) and dual-tree complex WT-based support vector machine (DTCWT-SVM) for comparisons purposes. In this, the accuracy of the WT-SOMN and DWT-ANN techniques was 91.27% and 97.7%, respectively, without being subjected to noise analysis. However, the proposed methods are evaluated under noise conditions and achieve a higher accuracy range than existing works. Here, the proposed method attained a high accuracy of 99.95% under noise conditions.

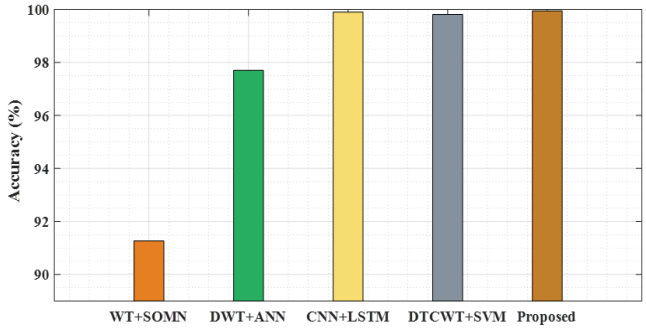

Figure 14: Accuracy comparisons with existing works with noise.

Table 2 represents the comparative analysis of accuracy with different methods and distributed systems. This comparison shows that the proposed model achieved high accuracy by using the proposed method.

Table 2: Comparative analysis of accuracy

Reference	Method	Bus system	Noise condition	Accuracy
[20]	WT+SOMN	IEEE-18	Not considered	91.27%
[21]	DWT+ANN	IEEE-38	Not considered	97.7%
[22]	CNN+LSTM	IEEE-13	Noise considered	99.90
[23]	DTCWT+SVM	IEEE-33	Noise considered	99.81%
Proposed	FBSE-EWT+ Bi-LSTM	IEEE-33	Noise considered	99.95%

NDZ is defined as the area where the proposed method fails to identify islanding condition. When assessing effectiveness of islanding detection techniques, the NDZ value is a crucial component. It is a functional zone where the islanding situation cannot be detected. Mostly, voltage limits are used as 1.1 p.u and for maximum - minimum as 0.9 p.u as per the distributed network of Malaysia. The frequency for distributed networks ranges between 49.5Hz and 50.5Hz.

Table 3: Comparative assessment of the proposed method

Method	Bus Number	NDZ	Time
[24]	IEEE 33	0.05 MW & 0.0.5 MVAR	100 -200ms
[25]	IEEE 33	0.03 MW & 0.03 MVAR	200ms
[26]	IEEE 33	0.01 MW & 0.01 MVAR	167ms
Proposed	IEEE 33	0	75ms

Table 3 represents the analysis for NDZ with existing works based on time and distributed network. For this comparison, only an IEEE 33-based distributed network was analyzed. The method in [24] has not detected 0.05 values, and it takes 200ms to detect islanding. However, the proposed method detected the entire island zone with a minimum duration of 75 ms. It was very time-saving and efficient compared to the existing method. Therefore, the proposed islanding detection approach efficiently reduced NDZ to zero and increased accuracy in islanding detection. Here, proposed method will accurately and effectively find islanding detection with the fault-affected zone.

5. Conclusion

In this work, an FBSE-EWT-based GAO-optimized Bi-LSTM method is proposed to detect islanding conditions. An adapted IEEE 33 bus through hybrid renewable resources for examining the proposed method. The FBSE-EWT method extracts the features to analyze the fault in a distributed system. Based on the extracted features, islanding faults are classified using Bi-LSTM. The weight parameter of this BI-LSTM is regulated by the GAO algorithm. The effectiveness of the proposed approach is thoroughly assessed in the MATLAB/Simulink environment under a wide range of operating scenarios. These include islanding conditions, sudden load changes, DG fluctuation and various fault disturbances, ensuring a comprehensive evaluation of system stability and controller robustness. Moreover, performance metrics like f1-score, recall, accuracy and precision is evaluated and analyzed with conventional methods. Comparative output gives high accuracy than the existing methods. The proposed algorithms

can detect islanding within 75ms. The f1-score, accuracy, precision, recall and specificity of proposed method are demonstrated as 99.82%, 100%, 99.95%, 99.89% and 99.99% under without-noise conditions. The results represent, proposed method is proficient in identifying islanding operations. In future, proposed method might be evaluated with many IEEE bus systems.

Reference

[1] Kim, Min-Sung, Raza Haider, Gyu-Jung Cho, Chul-Hwan Kim, Chung-Yuen Won, and Jong-Seo Chai. "Comprehensive review of islanding detection methods for distributed generation systems." Energies 12, no. 5 (2019): 837.
[2] Chang, Gary W., and Nguyen Cong Chinh. "Coyote optimization algorithm-based approach for strategic planning of photovoltaic distributed generation." IEEE Access 8 (2020): 36180-36190.
[3] Worku, Muhammed Y., Mohamed A. Hassan, and Mohamed A. Abido. "Real time energy management and control of renewable energy based microgrid in grid connected and island modes." Energies 12, no. 2 (2019): 276.
[4] Worku, Muhammed Y., Mohamed A. Hassan, Luqman S. Maraaba, and Mohammad A. Abido. "Islanding detection methods for microgrids: A comprehensive review." Mathematics 9, no. 24 (2021): 3174.
[5] Merino, Julia, Patricio Mendoza-Araya, Giri Venkataramanan, and Mustafa Baysal. "Islanding detection in microgrids using harmonic signatures." IEEE Transactions on Power Delivery 30, no. 5 (2014): 2102-2109.
[6] Raza, Safdar, Hazlie Mokhlis, Hamzah Arof, J. A. Laghari, and Li Wang. "Application of signal processing techniques for islanding detection of distributed generation in distribution network: A review." Energy Conversion and Management 96 (2015): 613-624.
[7] Shafique, Nouman, Safdar Raza, Sumayya Bibi, Muhammad Farhan, and Mughees Riaz. "A simplified passive islanding detection technique based on susceptible power indice with zero NDZ." Ain Shams Engineering Journal 13, no. 4 (2022): 101637.
[8] Bakhshi-Jafarabadi, Reza, and Javad Sadeh. "New voltage feedback-based islanding detection method for grid-connected photovoltaic systems of microgrid with zero non-detection zone." IET Renewable Power Generation 14, no. 10 (2020): 1710-1719.
[9] Elshrief, Yasser A., Sameh Abd-Elhaleem, Sulayman Kujabi, Dalal H. Helmi, Belal A. Abozalam, and Amin D. Asham. "Zero Non-Detection Zone for Islanding Detection Based on a Novel Hybrid Passive-Active Technique with Fuzzy Inference System." Sustainability 14, no. 10 (2022): 6325.
[10] Ashwin, K. V., Venkata Satya Rahul Kosuru, S. Sridhar, and P. Rajesh. "A Passive Islanding Detection Technique Based on Susceptible Power Indices with Zero Non-Detection Zone Using a Hybrid Technique." International Journal of Intelligent Systems and Applications in Engineering 11, no. 2 (2023): 635-647.
[11] Naraghipour, Kianoush, Ibrahim Abdelsalam, Khaled H. Ahmed, and Campbell D. Booth. "Modified Q–f droop curve method for islanding detection with zero non-detection zone." IEEE Access 9 (2021): 158027-158040.
[12] Pangedaiah, B., PL Santosh Kumar Reddy, Y. P. Obulesu, Venkata Reddy Kota, and Mamdouh L. Alghaythi. "A Robust Passive Islanding Detection Technique With Zero-Non-Detection Zone for Inverter-Interfaced Distributed Generation." IEEE Access 10 (2022): 96296-96306.
[13] Dolatabadi, Sarineh Hacopian, Maedeh Ghorbanian, Pierluigi Siano, and Nikos D. Hatziargyriou. "An enhanced IEEE 33 bus benchmark test system for distribution system studies." IEEE Transactions on Power Systems 36, no. 3 (2020): 2565-2572.

[14] Subramanian, Karthikeyan, and Ashok Kumar Loganathan. "Islanding detection using a micro-synchrophasor for distribution systems with distributed generation." Energies 13, no. 19 (2020): 5180.
[15] Buduma, Parusharamulu, Madan Kumar Das, Ramasamy Thaiyal Naayagi, Sukumar Mishra, and Gayadhar Panda. "Seamless operation of master-slave organized AC microgrid with robust control and islanding detection." In 2020 3rd International Conference on Energy, Power and Environment: Towards Clean Energy Technologies, pp. 1-6. IEEE, 2021.
[16] Alsabban, Maha, Otavio Bertozzi, and Shehab Ahmed. "Analysis and Verification of Islanding Detection Techniques for Grid-integrated PV Systems." In 2023 IEEE PES Conference on Innovative Smart Grid Technologies-Middle East (ISGT Middle East), pp. 1-5. IEEE, 2023.
[17] Fatimah, Binish, Amit Singhal, and Pushpendra Singh. "A multi-modal assessment of sleep stages using adaptive Fourier decomposition and machine learning." Computers in Biology and Medicine 148 (2022): 105877.
[18] Jahan, Sobhana, Farhana Nowsheen, Mahathir Mahmud Antik, Md Sazzadur Rahman, M. Shamim Kaiser, ASM Sanwar Hosen, and In-Ho Ra. "AI-based Epileptic Seizure Detection and Prediction in Internet of Healthcare Things: A Systematic Review." IEEE Access (2023).
[19] Dehghani, Mohammad, Pavel Trojovský, and Om Parkash Malik. "Green Anaconda Optimization: A New Bio-Inspired Metaheuristic Algorithm for Solving Optimization Problems." Biomimetics 8, no. 1 (2023): 121.
[20] Hong YY, Huang WS, Chang YR, Lee YD, Ouyang DC. Locating high-impedance fault in a smart distribution system using wavelet entropy and hybrid self-organizing mapping network. In: Proceedings of the 2017 IEEE PES Innovative Smart Grid Technologies Conference Europe; 2017:1-6.
[21] Ali MS, Bakar AH, Tan C. High impedance fault localization using discrete wavelet transform for single line to ground fault. Arab J Sci Eng. 2017;42:5031-5044.
[22] Vadlamudi, Bindu. "Optimized Hybrid CNN-LSTM Based Islanding Detection of Solar-Wind Power System." Electric Power Components and Systems (2023): 1-19.
[23] Joga, S. Ramana Kumar, Pampa Sinha, and Manoj Kumar Maharana. "A novel graph search and machine learning method to detect and locate high impedance fault zone in distribution system." Engineering Reports 5, no. 1 (2023): e12556.
[24] Raza, Safdar, H. Amjad, M. Umer, and A. Khalid. "Analysis of power system parameters for islanding detection using wavelet transform." Indonesian Journal of Electrical Engineering and Computer Science 17, no. 3 (2020): 1184-1193.
[25] Rostami, Ali, Amin Jalilian, Mehrdad Tarafdar Hagh, Kashem M. Muttaqi, and Javad Olamaei. "Islanding detection of distributed generation based on rate of change of exciter voltage with circuit breaker switching strategy." IEEE Transactions on Industry Applications 55, no. 1 (2018): 954-963.
[26] Abdi, Hamdi, Ali Rostami, and Navid Rezaei. "A novel passive islanding detection scheme for synchronous-type DG using load angle and mechanical power parameters." Electric Power Systems Research 192 (2021): 106968.